

A Multi-Stage Auto-Context Deep Learning Framework for Tissue and Nuclei Segmentation and Classification in H&E-Stained Histological Images of Advanced Melanoma

Nima Torbati^{1*}, Anastasia Meshcheryakova^{2*}, Diana Mechtcheriakova^{2**}, and Amirreza Mahbod^{1**}

¹ Research Center for Medical Image Analysis and Artificial Intelligence, Department of Medicine, Faculty of Medicine and Dentistry, Danube Private University, Austria

² Department of Pathophysiology and Allergy Research, Center of Pathophysiology, Infectiology and Immunology, Medical University of Vienna, Austria

Abstract. Melanoma is the most lethal form of skin cancer, with an increasing incidence rate worldwide. Analyzing histological images of melanoma by localizing and classifying tissues and cell nuclei is considered the gold standard method for diagnosis and treatment options for patients. While many computerized approaches have been proposed for automatic analysis, most perform tissue-based analysis and nuclei (cell)-based analysis as separate tasks, which might be suboptimal.

In this work, using the PUMA challenge dataset, we proposed a novel multi-stage deep learning approach by combining tissue and nuclei information in a unified framework based on the auto-context concept to perform segmentation and classification in histological images of melanoma. Through pre-training and further post-processing, our approach achieved second and first place rankings in the PUMA challenge, with average micro Dice tissue score and summed nuclei F1-score of 73.40% for Track 1 and 63.48% for Track 2, respectively. Our implementation for training and testing is available at: <https://github.com/NimaTorbati/PumaSubmit>

Keywords: Tissue Segmentation · Nuclei Segmentation · Medical Image Analysis · Machine Learning · Deep Learning · Melanoma · Computational Pathology.

1 Introduction

Skin cancer is one of the most common types of cancer, with melanoma being the most aggressive form [13]. Although many non-invasive approaches such as dermatoscopic or clinical image analysis are widely used for early detection [21,20,18], examination through biopsy and analysis of histological images remains the gold standard for diagnosis [4].

¹ * Equal contributions

² ** Equal contributions

Various staining methods exist for histological specimens, but hematoxylin and eosin (H&E) staining is the most commonly used by pathologists [8]. To categorize histological images, such as distinguishing between primary melanomas (referred to as primary in the rest of the text) and melanomas at distant metastatic sites (referred to as metastatic in the rest of the text), medical experts and pathologists can visually examine the slides and, based on their knowledge and experience, make diagnostic and treatment decisions. Several factors influence diagnostic accuracy, including the location and types of tissues and cells in the investigated specimens. Manual examination and assessment are labor-intensive and subject to intra- and inter-observer variability [28].

With the advancement of machine learning and deep learning, automated computer-based methods have become powerful tools for performing tissue and nuclei segmentation and classification [19]. These models can be trained using various approaches, including unsupervised, semi-supervised, self-supervised, and recently developed contrastive learning methods used in foundation model training [22,23,16]. However, the most accurate models are typically trained in a supervised manner, which requires annotated data.

For supervised training of tissue and nuclei segmentation and classification models, several publicly available datasets exist. Datasets such as BACH [2], GlaS [29], and CRAG [1] can be used for tissue segmentation. For nuclei segmentation and classification, datasets like PanNuke [5], NuInsSeg [15], MoNuSAC [32], and MoNuSeg [12] can be utilized.

In terms of model development, many approaches have been proposed for each task. Convolutional neural networks (CNNs)-based and vision transformer (ViT)-based models such as U-Net [24], U-Net++ [35], SegFormer [33,27], and nnU-Net [11,30] have been used for tissue segmentation in histological images. On the other hand, HoverNet [7], HoVer-Next [3], CellViT [10], CellViT++ [9], and DDU-Net [17] are examples of models developed specifically for nuclei instance segmentation and classification.

While these datasets and models have contributed significantly to the field of computational pathology, only a few focus on the combined task of simultaneous tissue and nuclei segmentation and classification. Examples of such efforts include the OCELOT challenge dataset [26] and the models proposed in [6,26]. However, these datasets and models are not specifically designed for histological image analysis of advanced melanoma.

To address this gap, the Panoptic segmentation of nUclei and tissue in advanced Melanoma (PUMA) challenge introduced a dataset specifically designed for simultaneous tissue and nuclei segmentation and classification in H&E-stained melanoma specimens. The challenge aims to provide a unique dataset and encourage the research community to develop robust models for two main tasks defined in its two tracks. Track 1 involves segmentation and classification of five tissue types and three nuclei instance types. Track 2 includes segmentation and classification of the same five tissue types and ten nuclei instance classes. It is important to note that the background class is not treated as a separate class in either track.

In this study, we proposed a novel multi-stage approach based on the auto-context concept [31] and participated in both tracks of the PUMA challenge. The results on the final test set confirmed the excellent performance of our method, achieving a mean micro Dice tissue score and summed nuclei F1-score of 73.40% for Track 1 and 63.48% for Track 2, respectively. These results ranked our approach (submitted under the name "LSM team") second in Track 1 and first in Track 2 of the PUMA competition, respectively ³.

2 Method

We proposed a multi-stage auto-context pipeline, where the outputs of earlier stages are used as contextual input to refine tissue segmentation and nuclei segmentation and classification in later stages. Our method consists of four main stages, as illustrated in Figure 1, Figure 2, Figure 3, and Figure 4.

In the first stage (Figure 1), we designed a classifier to determine the input image type, distinguishing between primary and metastatic frames. In the second stage (Figure 2), initial tissue segmentation is performed. The third stage (Figure 3) involves nuclei instance segmentation using the baseline HoVer-Next model, along with nuclei classification, which utilizes the tissue information from the previous step. Finally, in the fourth stage (Figure 4), tissue segmentation is refined using the nuclei masks produced in the third stage. Further explanation of our entire pipeline is described below.

2.1 Datasets

We used two datasets in this work: the PanopTILs dataset [14] and the PUMA dataset [28]. The former was used only for pre-training, while the latter was used for fine-tuning and participation in the PUMA challenge.

The PanopTILs dataset contains a total of 1,709 image patches extracted from whole-slide images. Each patch has a size of 1024×1024 pixels with an image resolution of 0.25 microns per pixel, which is approximately equivalent to $40\times$ magnification. Since the PUMA dataset images have a slightly different resolution (0.23 microns per pixel), we first cropped the PanopTILs images to 880×880 pixels (top-left cropping) and then resized them to 1024×1024 pixels to ensure a similar resolution comparable to that of the PUMA images. The PanopTILs dataset includes annotations for 9 tissue types (exclude, cancerous epithelium, stroma, TILs, normal epithelium, junk/debris (necrosis), blood, other, and white space/empty) and 10 nuclei types (exclude, cancer nucleus, stromal nucleus, large stromal nucleus, lymphocyte nucleus, plasma cell / large TIL nucleus, normal epithelial nucleus, other nucleus, unknown/ambiguous nucleus, and background). From the original 1,709 image regions, we used only 300 images for pre-training and merged some classes to align the labels more closely with those used in the PUMA dataset. In the case of tissue classes, we grouped

³ <https://puma.grand-challenge.org/>

"exclude," "other," and "white space/empty" as white background, while "cancerous epithelium" and "TILs" were grouped as tumor. Only images containing necrosis or tumor tissue were used in our analysis, while those containing the normal epithelium class were excluded.

The other dataset used in this study is the PUMA dataset [28], which served as the main dataset for our experiments. It contains a total of 310 melanoma image patches: 155 from primary tumors and 155 from metastatic tumors, all with a size of 1024×1024 pixels. These were divided into training (206 images), validation (10 images), and test (94 images) sets. While both tissue and nuclei annotations were provided for the training images, the labels for the validation and test images were kept private by the challenge organizers. Participants in the challenge could evaluate their models on the 10 validation images (also referred as preliminary test set in the challenge) through the PUMA Grand Challenge platform ⁴ and submit their final results for the 94 test images. The PUMA dataset includes annotations for six tissue types: tumor, stroma, epidermis, necrosis, blood vessel, and background. For nuclei, Track 1 of the challenge includes four types: tumor cells, lymphocyte, stroma cell, and other. Track 2 includes ten types: tumor cell, lymphocyte, plasma cell, histocyte, melanophage, neutrophil, stroma cell, endothelium, epithelium, and apoptotic cell, as well as the background class. In our experiments, we used all training images except one due to a mismatch between the image and the provided segmentation mask. Further details about the PUMA dataset can be found in [28].

It is worth mentioning that the flowcharts shown in the rest of the manuscript present only the fine-tuning steps with the PUMA dataset and do not include the pre-training with the PanopTILs dataset.

2.2 Utilized Backbone Models

In this study, we used four state-of-the-art segmentation models at different stages of our proposed method. The first model is SegFormer [33] (B2 variant) with ImageNet pre-trained weights [25]. The second model is U-Net [24] with a pre-trained ResNet34 encoder [34]. The third model is UNet++ [35] with a pre-trained ResNet50 encoder [34]. Finally, the fourth model is HoVer-Next, which was used exclusively for nuclei instance segmentation. The pre-trained HoVer-Next model, based on the PUMA training dataset, was provided by the challenge organizers.

2.3 Stage 1: Classifier

To address the challenges posed by the limited dataset size and variations in tissue types across skin and other organs, we differentiated tissue types between the primary and metastatic phases. Our approach involves training two separate models: one for primary images and another for metastatic images. Therefore, an initial classification step is required to determine the image type. To build the

⁴ <https://puma.grand-challenge.org/>

classifier, we first increased the number of tissue classes from five to ten, with the first five representing primary tissue types and the remaining five corresponding to metastatic tissue types. We then trained a SegFormer-B2 segmentation model with 11 classes (including the background) as the main classifier, followed by a set of handcrafted classification rules to categorize images as either primary or metastatic, as stated below.

An image is classified as primary if the segmentation result includes Epidermis. If the Epidermis is not present, the image is still classified as primary if the total number of primary pixels exceeds the total number of metastatic pixels. Otherwise, the image is classified as metastatic.

The flowchart of this stage is shown in Figure 1.

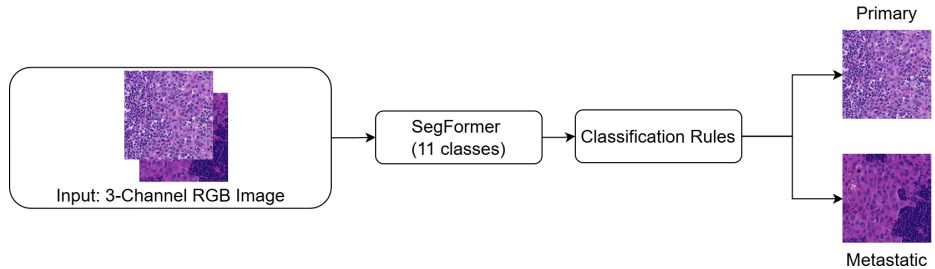


Fig. 1. The first stage of the proposed method: In the first stage of the proposed method, a SegFormer model is trained to classify the input image type (primary or metastatic) based on segmentation result and the classification rules.

2.4 Stage2: Initial Tissue Segmentation

In this stage, two SegFormer models are trained for initial tissue segmentation. One model is trained on the primary subset of the PUMA dataset, and the other is trained on the metastatic subset. Based on the classification results from stage 1, each input frame is directed to the appropriate model.

During our experiments, we observed that the performance of the SegFormer model in detecting blood vessel tissue was suboptimal. To address this, we trained a U-Net model using all available images in the PUMA dataset specifically for blood vessel detection. As a result, in our approach, we replaced the SegFormer predictions for blood vessel tissue with the corresponding U-Net predictions.

To further enhance the segmentation performance, we defined a set of tissue ensemble rules. The final prediction for epidermis and necrosis is computed as the average of the predictions from both SegFormer and U-Net models:

$$P_{\text{Epidermis}} = 0.5 (P_{\text{SegFormer_Epidermis}} + P_{\text{UNet_Epidermis}}) \quad (1)$$

$$P_{\text{Necrosis}} = 0.5 (P_{\text{SegFormer_Necrosis}} + P_{\text{UNet_Necrosis}}) \quad (2)$$

For blood vessel class, we directly use the U-Net output:

$$P_{\text{Blood vessel}} = P_{\text{UNet_Blood vessel}} \quad (3)$$

The predictions for tumor and stroma tissues are solely based on the SegFormer output:

$$P_{\text{Tumor}} = P_{\text{SegFormer_Tumor}} \quad (4)$$

$$P_{\text{Stroma}} = P_{\text{SegFormer_Stroma}} \quad (5)$$

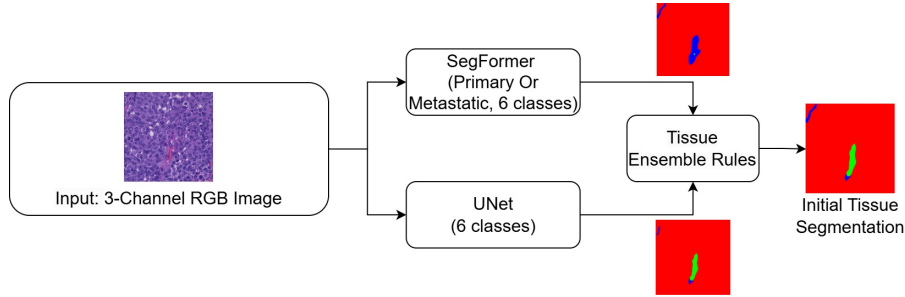


Fig. 2. The second stage of the proposed method: Initial tissue segmentation is performed using two SegFormer models, one for primary tissues and the other for metastatic tissues. Due to the Segformer model’s poor performance in segmenting blood vessel tissues, a U-Net model is trained separately for blood vessel detection and the results are refined using the tissue ensemble rules.

2.5 Stage3: Nuclei Segmentation

As shown in Figure 3, this stage consists of two branches: one for nuclei class map prediction and the other for nuclei instance segmentation. In the first branch, we incorporate the tissue segmentation result from stage 2 as a fourth input channel and train a U-Net++ model for nuclei class map prediction. In the second branch, nuclei instance masks are generated using the pre-trained HoVer-NeXt model [3], provided by the challenge organizers.

As observed in our experiments and inferred from the results in [28], rather than improving the instance segmentation outputs, we opted to use the baseline instance segmentation results from the HoVer-NeXt model and focused on enhancing the classification results using external models. Specifically, we employed U-Net++ with four input channels for this task. We previously tested this

approach (that is, using an external model solely for nuclei classification) in the MoNuSAC challenge, where we achieved first place on the post-challenge leaderboard [17,32]. In this study, for each detected instance from the HoVer-NeXt model, we determined the instance class from the U-Net++ predictions using a simple majority voting approach. The number of U-Net++ output classes depends on the challenge track: four classes for Track 1 and eleven classes for Track 2, including the background in both cases.

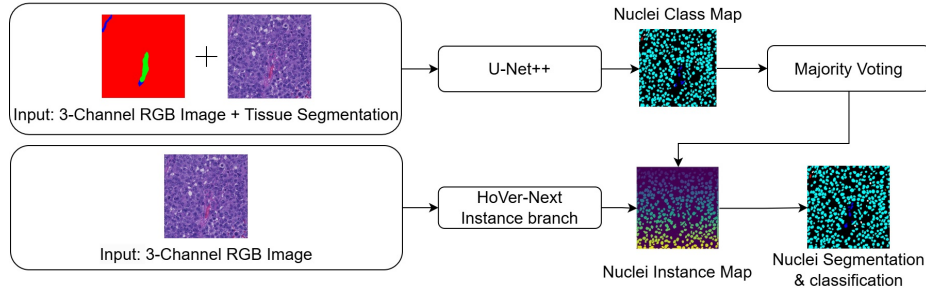


Fig. 3. The third stage of the proposed method consists of two branches for nuclei segmentation, utilizing tissue segmentation information. In the first branch, a U-Net++ model is trained for nuclei class map detection, incorporating tissue segmentation results as an additional input channel. In the second branch, nuclei instance segmentation is performed using the HoVer-NeXt model. The final nuclei segmentation and classification is obtained by combining the class maps and instance masks through a majority voting approach.

2.6 Stage4: Final Tissue segmentation

In this stage, we incorporate the nuclei segmentation result from stage 3 as a fourth input channel and three models similar to those in stage 2 are trained as shown in Figure 4. Tissue ensemble rules used in stage 4 are the same as in stage 2.

2.7 Post-Processing

To enhance the performance, we applied two post-processing steps to the tissue and nuclei segmentation results.

Tissue Post-Processing In stage 4, we observed under-segmentation of necrotic tissue. This issue arises due to the low density of nuclei in necrotic regions. An example of this under-segmentation is shown in Figure 5. To mitigate this, we incorporate predictions from stage 1 when there is an overlap between the stage 1 and stage 4 predictions for necrotic tissue. We applied this post-processing

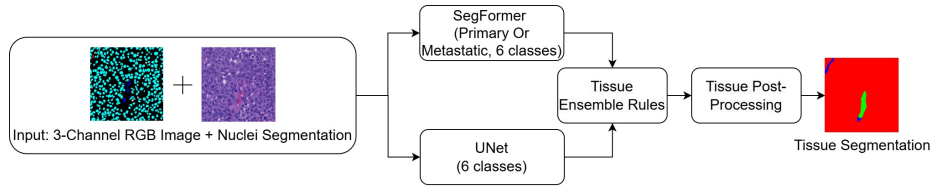


Fig. 4. The fourth and final stage of the proposed method: Tissue segmentation is refined using nuclei segmentation results. The nuclei segmentation output from the previous stage is added as an additional input channel, and three models similar to those in stage 2 are trained for this task.

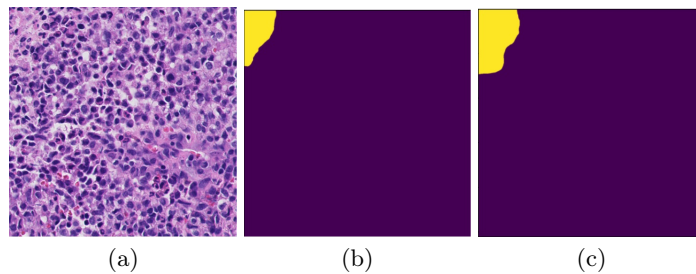


Fig. 5. Due to the low density of nuclei in necrotic tissue (a), the final segmentation result in stage 4 may suffer from under-segmentation (b). To address this, a post-processing step integrates predictions from stage 1 when they overlap with stage 4 predictions for necrotic tissue (c).

step only in Track 2 of the challenge and not in Track 1. As the results confirm, this post-processing significantly improved the tissue segmentation performance, especially for necrosis (refer to Table 1, Table 2, and Table 3 for further details).

Nuclei Post-Processing For nuclei segmentation, corrections are required for the instance segmentation map at image borders. Since HoVer-NeXt divides the input image into small patches during the inference phase, its performance at image borders is suboptimal. An example of this issue is shown in Figure 6. To address this, we replace the instance segmentation results at image borders with the corresponding class map results.

2.8 Evaluation

To evaluate the performance of the algorithms, the micro Dice score (for multi-class tissue segmentation) and the summed macro F1-score (for nuclei instance detection and classification) were used. The micro Dice score is calculated by treating all segmentation results from all images as a single large image. The summed macro F1-score is determined using a 15-pixel centroid threshold between the predicted segmentation of the nuclei results and the ground truth. For

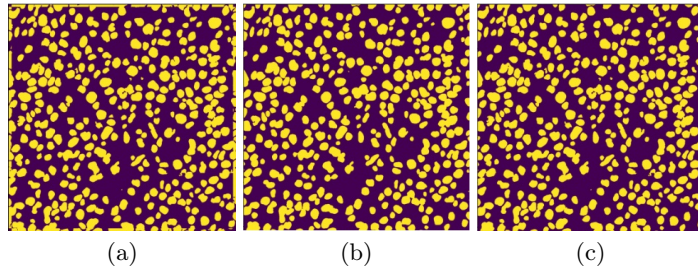


Fig. 6. At image borders, nuclei instance segmentation results are replaced with class map results. (a) Binary segmentation map from HoVer-Next. (b) Binary class map from U-Net ++. (c) Binary map after border correction.

the final ranking of the challenge, the average of the micro Dice score and the summed macro F1-score was used for both Track 1 and Track 2. Further details and implementation of the utilized metrics are available in the PUMA challenge description⁵.

3 Experiments

To conduct experiments, we utilized both transfer learning (as described in Section 2.1) and data augmentation techniques to improve the performance of the models. For data augmentation, we applied both shape-based transformations (flip, rotation, scaling) and intensity-based adjustments (hue, saturation, brightness, contrast). All experiments were conducted using a single workstation with AMD Ryzen 9 7950X CPU, 96 GB of RAM, and two NVIDIA RTX 4090 GPUs. Our implementation for training and testing is available on our GitHub repository: <https://github.com/NimaTorbati/PumaSubmit>.

4 Results & Discussion

The final test results and rankings of Track 1 and Track 2 for the top three performers in the PUMA challenge, as well as the baseline results provided by the challenge organizers (nnU-Net [11] for tissue segmentation and HoVer-NeXt [3] for nuclei segmentation and classification), are shown in Table 1 and Table 2, respectively.

As the results show, all three top-ranked teams outperformed the provided baseline method by a large margin. Details of the methods used by the other top-performing teams (i.e., TIAKong, rictoo, and agaldran) are not available at the time of writing this manuscript but are expected to be released by the organizers. With our proposed approach (LSM), we achieved second place in Track 2 and first place in Track 1 of the competition.

⁵ <https://puma.grand-challenge.org/submission/>

When considering only the performance for nuclei instance segmentation and classification, we achieved the best performance in Track 1 and the second-best performance in Track 2. However, for multi-class tissue segmentation, our method ranked third in Track 1 and second in Track 2.

Table 1. The final test results and ranking of Track 1 of the PUMA challenge.

Rank	Team	Micro Dice (Tissue)(%)	Summed macro F1 (Nuclei) (%)	Mean (%)
1	TIAKong	78.23	74.39	76.31
2	LSM	72.37	74.43	73.40
3	rictoo	63.26	75.78	69.52
8	Baseline	55.48	69.40	62.44

Table 2. The final test results and ranking of Track 2 of the PUMA challenge.

Rank	Team	Micro Dice (Tissue)(%)	Summed macro F1 (Nuclei) (%)	Mean (%)
1	LSM	77.98	48.97	63.48
2	TIAKong	78.23	46.69	62.46
3	agaldran	62.04	47.78	54.91
11	Baseline	55.48	29.77	42.63

As pointed out in Section 2.7, we only applied the proposed tissue segmentation post processing in Track 2 of the challenge. As the average results indicate, this step significantly improved overall performance. We also report the tissue-specific scores on the final test sets of Track 1 and Track 2 in Table 3. According to these results, the post processing step notably enhanced the segmentation performance for necrosis tissue (from 46.69% to 74.49%). However, it should be noted that necrosis is the least represented tissue across the training, validation, and test sets. Therefore, even small over- or under-segmentation can significantly affect the micro Dice score for necrosis, and thus influence the overall average tissue segmentation performance.

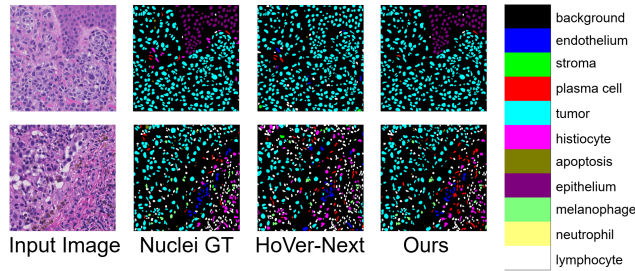
In Table 3, we also compare our tissue-specific performance with that of the top-performing team (TIAKong). As the results show, our method outperforms TIAKong for epidermis and blood vessel tissue segmentation, while TIAKong delivers better results for the remaining tissue types on the final test set.

It should be noted that the summed F1-score for each nuclei type is not provided by the challenge organizers; only the average results are reported as shown in Table 1 and Table 2. When this information becomes available, we will include it in the updated version of the manuscript. However, in Figure 7, we show an example result of our approach and compare it with the baseline HoVer-Next and the ground truth segmentation mask. As the qualitative results

Table 3. Tissue-based scores for Track 1 and Track 2 of the challenge on the final test set, based on the micro Dice score (%).

Track	Team	Tumor	Stroma	Necrosis	Epidermis	Blood vessel	Mean
Track 1	LSM	92.07	81.28	46.79	87.32	54.37	72.37
Track 2	LSM	92.45	81.28	74.49	87.32	54.37	77.98
Track 1/2	TIAKong	93.57	83.59	82.03	86.25	45.69	78.23

clearly show, our predicted segmentation mask is much closer to the ground truth compared to the baseline HoVer-Next.

**Fig. 7.** Nuclei segmentation and classification result example

Further detailed results, including our internal and external validation as well as findings from the ablation study demonstrating the impact of each stage and the tissue and nuclei post processing steps, will also be added to the updated version of this manuscript in the near future.

5 Conclusion

In this work, we introduced a novel multi-stage auto-context deep learning framework to perform tissue and nuclei segmentation and classification in H&E-stained histological images of advanced melanoma. By exploiting contextual information across stages and integrating multiple state-of-the-art segmentation models, our method achieved excellent performance in the PUMA Challenge, ranking second in Track 1 and first in Track 2 of the competition. These results confirm the effectiveness of combining tissue and nuclei information in a unified framework. In future work, we plan to evaluate the performance of the proposed method on an external dataset and report the impact of each stage on the final performance through a comprehensive ablation study.

Acknowledgment

This work was supported by the Vienna Science and Technology Fund (WWTF) and by the State of Lower Austria [Grant ID: 10.47379/LS23006].

References

1. Alemi Koohbanani, N., Jahanifar, M., Zamani Tajadin, N., Rajpoot, N.: NuClick: A deep learning framework for interactive segmentation of microscopic images. *Medical Image Analysis* **65**, 101771 (2020). <https://doi.org/https://doi.org/10.1016/j.media.2020.101771>
2. Aresta, G., Araújo, T., Kwok, S., Chennamsetty, S.S., Safwan, M., Alex, V., Marami, B., Prastawa, M., Chan, M., Donovan, M., Fernandez, G., Zeineh, J., Kohl, M., Walz, C., Ludwig, F., Braunewell, S., Baust, M., Vu, Q.D., To, M.N.N., Kim, E., Kwak, J.T., Galal, S., Sanchez-Freire, V., Brancati, N., Frucci, M., Riccio, D., Wang, Y., Sun, L., Ma, K., Fang, J., Kone, I., Boulmane, L., Campilho, A., Eloy, C., Polónia, A., Aguiar, P.: BACH: Grand challenge on breast cancer histology images. *Medical Image Analysis* **56**, 122–139 (2019). <https://doi.org/https://doi.org/10.1016/j.media.2019.05.010>
3. Baumann, E., Dislich, B., Rumberger, J.L., Nagtegaal, I.D., Martinez, M.R., Zlobec, I.: Hover-next: A fast nuclei segmentation and classification pipeline for next generation histopathology. In: Burgos, N., Petitjean, C., Vakalopoulou, M., Christodoulidis, S., Coupe, P., Delingette, H., Lartizien, C., Mateus, D. (eds.) *Proceedings of The 7nd International Conference on Medical Imaging with Deep Learning. Proceedings of Machine Learning Research*, vol. 250, pp. 61–86. PMLR (2024)
4. Elmore, J.G., Barnhill, R.L., Elder, D.E., Longton, G.M., Pepe, M.S., Reisch, L.M., Carney, P.A., Titus, L.J., Nelson, H.D., Omega, T., Tosteson, A.N.A., Weinstock, M.A., Knezevich, S.R., Piepkorn, M.W.: Pathologists’ diagnosis of invasive melanoma and melanocytic proliferations: observer accuracy and reproducibility study. *BMJ* **357** (2017). <https://doi.org/https://doi.org/10.1136/bmj.j2813>
5. Gamper, J., Alemi Koohbanani, N., Benet, K., Khuram, A., Rajpoot, N.: Pan-Nuke: An open pan-cancer histology dataset for nuclei instance segmentation and classification. In: Reyes-Aldasoro, C.C., Janowczyk, A., Veta, M., Bankhead, P., Sirinukunwattana, K. (eds.) *Digital Pathology*. pp. 11–19. Springer International Publishing, Cham (2019). https://doi.org/https://doi.org/10.1007/978-3-030-23937-4_2
6. Graham, S., Vu, Q.D., Jahanifar, M., Raza, S.E.A., Minhas, F., Snead, D., Rajpoot, N.: One model is all you need: Multi-task learning enables simultaneous histology image segmentation and classification. *Medical Image Analysis* **83**, 102685 (2023). <https://doi.org/https://doi.org/10.1016/j.media.2022.102685>
7. Graham, S., Vu, Q.D., Raza, S.E.A., Azam, A., Tsang, Y.W., Kwak, J.T., Rajpoot, N.: Hover-Net: Simultaneous segmentation and classification of nuclei in multi-tissue histology images. *Medical Image Analysis* **58**, 101563 (2019). <https://doi.org/https://doi.org/10.1016/j.media.2019.101563>
8. de Haan, K., Zhang, Y., Zuckerman, J.E., Liu, T., Sisk, A.E., Diaz, M.F.P., Jen, K.Y., Nobori, A., Liou, S., Zhang, S., Riahi, R., Rivenson, Y., Wallace, W.D., Ozcan, A.: Deep learning-based transformation of h&e stained tissues into special stains. *Nature Communications* **12**(1), 4884 (2021). <https://doi.org/https://doi.org/10.1038/s41467-021-25221-2>

9. Hörst, F., Rempe, M., Becker, H., Heine, L., Keyl, J., Kleesiek, J.: Cellvit++: Energy-efficient and adaptive cell segmentation and classification using foundation models. arXiv preprint arXiv:2501.05269 (2025)
10. Hörst, F., Rempe, M., Heine, L., Seibold, C., Keyl, J., Baldini, G., Ugurel, S., Siveke, J., Grünwald, B., Egger, J., Kleesiek, J.: Cellvit: Vision transformers for precise cell segmentation and classification. *Medical Image Analysis* **94**, 103143 (2024). <https://doi.org/https://doi.org/10.1016/j.media.2024.103143>
11. Isensee, F., Jaeger, P.F., Kohl, S.A.A., Petersen, J., Maier-Hein, K.H.: nnu-net: a self-configuring method for deep learning-based biomedical image segmentation. *Nature Methods* **18**(2), 203–211 (2021). <https://doi.org/https://doi.org/10.1038/s41592-020-01008-z>
12. Kumar, N., Verma, R., Anand, D., Zhou, Y., Onder, O.F., Tsougenis, E., Chen, H., Heng, P.A., Li, J., Hu, Z., Wang, Y., Koohbanani, N.A., Jahanifar, M., Tajeddin, N.Z., Gooya, A., Rajpoot, N., Ren, X., Zhou, S., Wang, Q., Shen, D., Yang, C.K., Weng, C.H., Yu, W.H., Yeh, C.Y., Yang, S., Xu, S., Yeung, P.H., Sun, P., Mahbod, A., Schaefer, G., Ellinger, I., Ecker, R., Smedby, O., Wang, C., Chidester, B., Ton, T.V., Tran, M.T., Ma, J., Do, M.N., Graham, S., Vu, Q.D., Kwak, J.T., Gunda, A., Chunduri, R., Hu, C., Zhou, X., Lotfi, D., Safdari, R., Kascenas, A., O’Neil, A., Eschweiler, D., Stegmaier, J., Cui, Y., Yin, B., Chen, K., Tian, X., Gruening, P., Barth, E., Arbel, E., Remer, I., Ben-Dor, A., Sirazitdinova, E., Kohl, M., Braunewell, S., Li, Y., Xie, X., Shen, L., Ma, J., Baksi, K.D., Khan, M.A., Choo, J., Colomer, A., Naranjo, V., Pei, L., Iftekharuddin, K.M., Roy, K., Bhattacharjee, D., Pedraza, A., Bueno, M.G., Devanathan, S., Radhakrishnan, S., Koduganty, P., Wu, Z., Cai, G., Liu, X., Wang, Y., Sethi, A.: A multi-organ nucleus segmentation challenge. *IEEE Transactions on Medical Imaging* **39**(5), 1380–1391 (2020). <https://doi.org/https://doi.org/10.1109/TMI.2019.2947628>
13. Leiter, U., Eigentler, T., Garbe, C.: Epidemiology of skin cancer. In: *Sunlight, Vitamin D and Skin Cancer*, pp. 120–140. Springer (2014). https://doi.org/https://doi.org/10.1007/978-1-4939-0437-2_7
14. Liu, S., Amgad, M., More, D., Rathore, M.A., Salgado, R., Cooper, L.A.D.: A panoptic segmentation dataset and deep-learning approach for explainable scoring of tumor-infiltrating lymphocytes. *npj Breast Cancer* **10**(1), 52 (2024). <https://doi.org/https://doi.org/10.1038/s41523-024-00663-1>
15. Mahbod, A., Polak, C., Feldmann, K., Khan, R., Gelles, K., Dorffner, G., Woitek, R., Hatamikia, S., Ellinger, I.: Nuinsseg: A fully annotated dataset for nuclei instance segmentation in h&e-stained histological images. *Scientific Data* **11**(1), 295 (2024). <https://doi.org/https://doi.org/10.1038/s41597-024-03117-2>
16. Mahbod, A., Saeidi, N., Hatamikia, S., Woitek, R.: Evaluating pre-trained convolutional neural networks and foundation models as feature extractors for content-based medical image retrieval. *Engineering Applications of Artificial Intelligence* **150**, 110571 (2025). <https://doi.org/https://doi.org/10.1016/j.engappai.2025.110571>
17. Mahbod, A., Schaefer, G., Dorffner, G., Hatamikia, S., Ecker, R., Ellinger, I.: A dual decoder u-net-based model for nuclei instance segmentation in hematoxylin and eosin-stained histological images. *Frontiers in Medicine* **9** (2022). <https://doi.org/https://doi.org/10.3389/fmed.2022.978146>
18. Mahbod, A., Schaefer, G., Wang, C., Ecker, R., Dorffner, G., Ellinger, I.: Investigating and exploiting image resolution for transfer learning-based skin lesion classification. In: *International Conference on Pattern Recognition*. pp. 4047–4053 (2021). <https://doi.org/https://doi.org/10.1109/ICPR48806.2021.9412307>

19. Nasir, E.S., Parvaiz, A., Fraz, M.M.: Nuclei and glands instance segmentation in histology images: a narrative review. *Artificial Intelligence Review* **56**(8), 7909–7964 (2023). <https://doi.org/https://doi.org/10.1007/s10462-022-10372-5>
20. Nie, Y., Sommella, P., Carratù, M., Ferro, M., O’Nils, M., Lundgren, J.: Recent advances in diagnosis of skin lesions using dermoscopic images based on deep learning. *IEEE Access* **10**, 95716–95747 (2022). <https://doi.org/https://doi.org/10.1109/ACCESS.2022.3199613>
21. Olayah, F., Senan, E.M., Ahmed, I.A., Awaji, B.: Ai techniques of dermoscopy image analysis for the early detection of skin lesions based on combined cnn features. *Diagnostics* **13**(7) (2023). <https://doi.org/https://doi.org/10.3390/diagnostics13071314>
22. Qu, L., Liu, S., Liu, X., Wang, M., Song, Z.: Towards label-efficient automatic diagnosis and analysis: a comprehensive survey of advanced deep learning-based weakly-supervised, semi-supervised and self-supervised techniques in histopathological image analysis. *Physics in Medicine & Biology* **67**(20), 20TR01 (2022). <https://doi.org/https://doi.org/10.1088/1361-6560/ac910a>
23. Raza, K., Singh, N.K.: A tour of unsupervised deep learning for medical image analysis. *Current Medical Imaging* **17**(9), 1059–1077 (2021). <https://doi.org/https://doi.org/10.2174/1573405617666210127154257>
24. Ronneberger, O., Fischer, P., Brox, T.: U-Net: Convolutional networks for biomedical image segmentation. In: *International Conference on Medical Image Computing and Computer-Assisted Intervention*. pp. 234–241 (2015). https://doi.org/https://doi.org/10.1007/978-3-319-24574-4_28
25. Russakovsky, O., Deng, J., Su, H., Krause, J., Satheesh, S., Ma, S., Huang, Z., Karpathy, A., Khosla, A., Bernstein, M., Berg, A.C., Fei-Fei, L.: Imagenet large scale visual recognition challenge. *International Journal of Computer Vision* **115**(3), 211–252 (2015). <https://doi.org/https://doi.org/10.1007/s11263-015-0816-y>
26. Ryu, J., Puche, A.V., Shin, J., Park, S., Brattoli, B., Lee, J., Jung, W., Cho, S.I., Paeng, K., Ock, C.Y., Yoo, D., Pereira, S.: Ocelot: Overlapped cell on tissue dataset for histopathology. In: *Proceedings of the IEEE/CVF Conference on Computer Vision and Pattern Recognition (CVPR)*. pp. 23902–23912 (June 2023)
27. Saleena, T., Ilyas, P.M., M Kutty, S.V.: Segformer-based approach for semantic segmentation of necrotic tissues from histopathology images. In: *2024 IEEE International Conference on Distributed Computing, VLSI, Electrical Circuits and Robotics (DISCOVER)*. pp. 383–387 (2024). <https://doi.org/https://doi.org/10.1109/DISCOVER62353.2024.10750697>
28. Schuiveling, M., Liu, H., Eek, D., Breimer, G.E., Suijkerbuijk, K.P.M., Blokx, W.A.M., Veta, M.: A novel dataset for nuclei and tissue segmentation in melanoma with baseline nuclei segmentation and tissue segmentation benchmarks. *GigaScience* **14**, giaf011 (2025). <https://doi.org/https://doi.org/10.1093/gigascience/giaf011>
29. Sirinukunwattana, K., Pluim, J.P., Chen, H., Qi, X., Heng, P.A., Guo, Y.B., Wang, L.Y., Matuszewski, B.J., Bruni, E., Sanchez, U., Böhm, A., Ronneberger, O., Cheikh, B.B., Racoceanu, D., Kainz, P., Pfeiffer, M., Urschler, M., Snead, D.R., Rajpoot, N.M.: Gland segmentation in colon histology images: The glas challenge contest. *Medical Image Analysis* **35**, 489–502 (2017). <https://doi.org/https://doi.org/10.1016/j.media.2016.08.008>
30. Spronck, J., Gelton, T., van Eekelen, L., Bogaerts, J., Tessier, L., van Rijthoven, M., van der Woude, L., van den Heuvel, M., Theelen, W., van der Laak, J., Ciompi, F.:

- nnunet meets pathology: Bridging the gap for application to whole slide images and computational biomarkers. In: Oguz, I., Noble, J., Li, X., Styner, M., Baumgartner, C., Rusu, M., Heinmann, T., Kontos, D., Landman, B., Dawant, B. (eds.) *Medical Imaging with Deep Learning*. Proceedings of Machine Learning Research, vol. 227, pp. 1859–1874. PMLR (2024)
31. Tu, Z., Bai, X.: Auto-context and its application to high-level vision tasks and 3d brain image segmentation. *IEEE Transactions on Pattern Analysis and Machine Intelligence* **32**(10), 1744–1757 (2010). <https://doi.org/https://doi.org/10.1109/TPAMI.2009.186>
 32. Verma, R., Kumar, N., Patil, A., Kurian, N.C., Rane, S., Graham, S., Vu, Q.D., Zwager, M., Raza, S.E.A., Rajpoot, N., Wu, X., Chen, H., Huang, Y., Wang, L., Jung, H., Brown, G.T., Liu, Y., Liu, S., Jahromi, S.A.F., Khani, A.A., Montahaei, E., Baghshah, M.S., Behroozi, H., Semkin, P., Rassadin, A., Dutande, P., Lodaya, R., Baid, U., Baheti, B., Talbar, S., Mahbod, A., Ecker, R., Ellinger, I., Luo, Z., Dong, B., Xu, Z., Yao, Y., Lv, S., Feng, M., Xu, K., Zunair, H., Hamza, A.B., Smiley, S., Yin, T.K., Fang, Q.R., Srivastava, S., Mahapatra, D., Trnavska, L., Zhang, H., Narayanan, P.L., Law, J., Yuan, Y., Tejomay, A., Mitkari, A., Koka, D., Ramachandra, V., Kini, L., Sethi, A.: MoNuSAC2020: A multi-organ nuclei segmentation and classification challenge. *IEEE Transactions on Medical Imaging* pp. 1–1 (2021). <https://doi.org/https://doi.org/10.1109/TMI.2021.3085712>
 33. Xie, E., Wang, W., Yu, Z., Anandkumar, A., Alvarez, J.M., Luo, P.: Segformer: Simple and efficient design for semantic segmentation with transformers. *Advances in neural information processing systems* **34**, 12077–12090 (2021)
 34. Yakubovskiy, P.: Segmentation models (2019), https://github.com/qubvel/segmentation_models
 35. Zhou, Z., Rahman Siddiquee, M.M., Tajbakhsh, N., Liang, J.: Unet++: A nested u-net architecture for medical image segmentation. In: Stoyanov, D., Taylor, Z., Carneiro, G., Syeda-Mahmood, T., Martel, A., Maier-Hein, L., Tavares, J.M.R., Bradley, A., Papa, J.P., Belagiannis, V., Nascimento, J.C., Lu, Z., Conjeti, S., Moradi, M., Greenspan, H., Madabhushi, A. (eds.) *Deep Learning in Medical Image Analysis and Multimodal Learning for Clinical Decision Support*. pp. 3–11. Springer International Publishing, Cham (2018). https://doi.org/https://doi.org/10.1007/978-3-030-00889-5_1